Final Technical Report

Project Title:

Oil-Impregnated Oxide Nanostructures for Aluminum Corrosion Prevention

Award No.: N00014-14-1-0502

Project Period: 6/1/14-9/30/17

Funding Amount: $361,260

Principal Investigator: Prof. Chang-Hwan Choi

Department of Mechanical Engineering

Stevens Institute of Technology

Castle Point on Hudson

Hoboken, NJ 07030

Phone: 201-216-5579

Fax: 201-216-8315

E-mail: cchoi@stevens.edu

REPORT DOCUMENTATION PAGE

Form Approved
OMB No. 0704-0188

1. REPORT DATE *(DD-MM-YYYY)*	2. REPORT TYPE	3. DATES COVERED *(From - To)*
18-12-2017	Final	6/1/2014 - 9/30/2017

4. TITLE AND SUBTITLE
Oil-Impregnated Oxide Nanostructures for Aluminum Corrosion Prevention

5a. CONTRACT NUMBER

5b. GRANT NUMBER
N00014-14-1-0502

5c. PROGRAM ELEMENT NUMBER

6. AUTHOR(S)
Choi, Chang-Hwan

5d. PROJECT NUMBER

5e. TASK NUMBER

5f. WORK UNIT NUMBER

7. PERFORMING ORGANIZATION NAME(S) AND ADDRESS(ES)
Stevens Institute of Technology
One Castle Point on Hudson
Hoboken, NJ 07030

8. PERFORMING ORGANIZATION REPORT NUMBER

9. SPONSORING/MONITORING AGENCY NAME(S) AND ADDRESS(ES)
ONR REG BOSTON N62879
495 Summer Street Room 627
Boston, MA 02210-2109

10. SPONSOR/MONITOR'S ACRONYM(S)

11. SPONSOR/MONITOR'S REPORT NUMBER(S)

12. DISTRIBUTION/AVAILABILITY STATEMENT
Approved for Public Release; Distribution is Unlimited

13. SUPPLEMENTARY NOTES

14. ABSTRACT
The major drawback of current passivation techniques for preventing corrosion is the lack of the ability to withstand any external damages or local defects. We have developed an oil-impregnated nanoporous anodic aluminum oxide (AAO) layer that can overcome such limitations and so advances corrosion protection.

15. SUBJECT TERMS
Corrosion, Aluminum

16. SECURITY CLASSIFICATION OF:			17. LIMITATION OF ABSTRACT	18. NUMBER OF PAGES	19a. NAME OF RESPONSIBLE PERSON
a. REPORT	b. ABSTRACT	c. THIS PAGE			19b. TELEPHONE NUMBER *(Include area code)*
U	U	U	SAR		

1. MOTIVATION AND OBJECTVIES

Aluminum and its alloys are one of the most promising metallic materials to reduce the weight of a mobile metal product, which is necessary for minimizing the CO_2 emission and maximizing fuel efficiency[1]. Nevertheless, due to the high reactivity of aluminum with oxygen and corrosive media, the application of aluminum can be restricted or some surface treatments to improve the corrosion resistance are required in some environments. Various strategies to prevent or mitigate the aluminum corrosion, such as cathodic protection, electroplating, conversion coating, anodizing, and polymer coating, have been widely demonstrated[2-7]. Among these techniques, anodizing (or anodic oxidation) is regarded as one of the most effective methods to protect aluminum from corrosion by forming an oxide passivation layer on top of the aluminum surface. However, since the anodic aluminum oxide (AAO) layer is composed of a thin barrier layer followed by a thick porous layer[8-10], the thick porous layer with high-aspect-ratio cylindrical pores is prone to absorb and retain corrosive media within the pores[11-13]. Thus, various methods have further been proposed to effectively seal the pores so that the corrosive media may not attack the thin barrier layer and penetrate the underlying metal surface.

Recently, hydrophobic coatings on textured hydrophilic metallic surfaces have been shown to improve corrosion resistance, making the surfaces superhydrophobic[14-18]. Such a superhydrophobicity allows the surface to minimize the contact area with a corrosive liquid, thus the absorption of the corrosive medium into the solid surface can be significantly impeded[14, 19]. However, there remain several issues in using superhydrophobic surfaces for anti-corrosion. First, the entrapped air in the hydrophobic structures is prone to be depleted due to thermodynamic and hydrodynamic effects, which cause the loss of the underlying air layer.[14, 20] In addition, the air-entrained composite interface can be broken easily or collapsed by localized damages, resulting in exposure of the metallic surface to the outer corrosive environment, typically without any self-repairing capability against the loss of air. In particular, fractured surfaces such as cracks, which are generated by vibration or thermal shock, are no longer hydrophobic, thus are prone to serve as penetration paths of corrosive medium toward the metallic substrate.[12, 21] This issue is not limited to the air-entrained hydrophobic surface, but also is a general problem for nanoporous AAO layer sealed with oxide materials.[11, 22]

Oil-impregnated surfaces, partly inspired by nature's *Nepenthes* pitcher plant, have recently been considered as a promising technology for multi-functional surfaces, having water-repellency, anti-icing, and anti-fouling capabilities.[23-29] Such an oil-infused surface forms a solid/oil/water composite interface unlike the conventional superhydrophobic surface forming a solid/air/water interface.[30-32] Impregnated oil not only minimizes the direct contact of water with the solid structures, but also has fluidity owing to the nature of oil, thus can allow unique self-cleaning and healing properties.[24, 33-36] In addition, the oil has thermodynamically and energetically more favorable affinity to a hydrophobic surface than water so that if oil is impregnated into the properly textured (e.g., nanostructured) hydrophobic surfaces, it will be kept stable and protect the surface from water or moisture more efficiently than conventional (air-impregnated) superhydrophobic surfaces.

The main objective of this project has been to investigate how the oil impregnated in the nanopores of anodic aluminum oxide would affect the corrosion resistance of aluminum and self-healing capability. **Figure 1** illustrates the key idea proposed in this research, i.e., employing *oil* instead of *air* for the interfacial water-repelling and corrosion-preventing layer. The oil completely impregnated in the nanopores of anodic oxide layer not only improves the corrosion resistance to

corrosive media but also automatically covers the exposed metallic aluminum surface by the presence of surface damage, so that the surface has an exceptional corrosion tolerance to physical damage and defects on the surface. To fully impregnate oil into the high-aspect-ratio dead-end nanopores of the anodized oxide layer of aluminum, we have developed a "solvent exchange method," which involves sequential exchange of solvents to ensure that the oil is fully infused into the pores. Moreover, to facilitate the oil impregnation, we have made the AAO surface hydrophobic. Due to the higher affinity of oil with the hydrophobic surface, the oil impregnated into the hydrophobic AAO layer is kept stable and can protect the surface from the aqueous corrosive media in a more efficient and durable way than air-impregnated hydrophobic surfaces. Then, we have investigated the corrosion inhibition properties of the oil-impregnated AAO layer, and compared with the conventional air-impregnated AAO layer. Furthermore, we have demonstrated superior durability and self-healing capability of the completely oil-impregnated AAO layer enabled by the solvent exchange method.

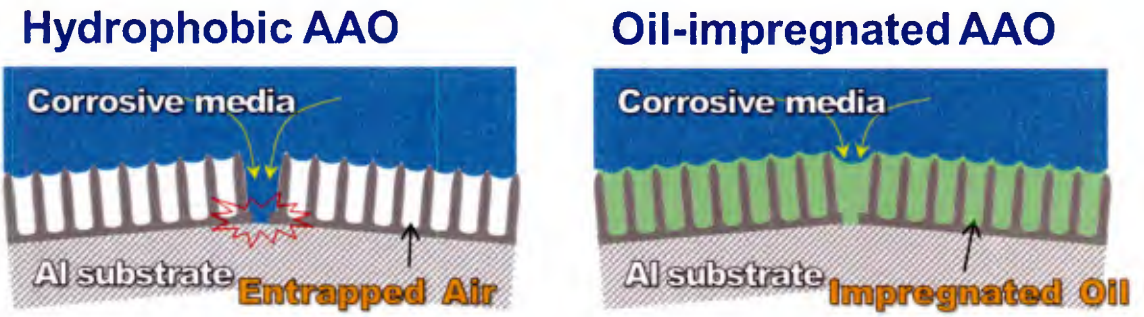

Figure 1. Paradigm shift from conventional "air"-entrained hydrophobic surfaces to novel "oil"-impregnated water-repelling surface and the self-healing mechanism of oil-impregnated anodic aluminum oxide (AAO).

2. RESULTS AND DISCUSSION

2.1. Fabrication of oil-impregnated nanoporous oxide layer using solvent exchange method

The fabricated AAO surface with cylindrical nanopores produced by anodization is shown in **Figures 2a-d**. Highly-ordered AAO nanopore structures with pore diameter of 70 nm and pore depth of 500 nm were created on the aluminum substrate by the anodization process. The scanning electron microscope (SEM) images of the AAO surface before and after the spin-coating of Teflon (**Figures 2b** and **2d**) do not show any significant difference in pore size. Considering the resolution of the SEM (~5 nm), the insignificant difference indicates the coating thickness of the Teflon onto the AAO surface could not be more than 5 nm, which agrees well with the measurement by ellipsometry (film thickness of ~2 nm) conducted on a smooth silicon surface.

The apparent contact angles of oil droplets (~3 μl) on various surfaces such as electropolished (bare) aluminum (Al), Teflon-coated aluminum (T-Al) after the electropolishing, anodic aluminum oxide (AAO), and Teflon-coated AAO (T-AAO) surfaces are presented in **Figure 2e**. The Krytox GPL 100 oil has a low surface tension (16-20 $mN \cdot m^{-1}$), thus spreads over the Al and AAO surfaces relatively easily, and exhibits low contact angles of 22±3° and 19±3°, respectively. In the presence of the hydrophobic Teflon coating on top of the surfaces, the contact angles of oil droplets were decreased to 4±1° and 5±1° for the Teflon-coated Al (T-Al) and AAO

(T-AAO), respectively. The reduced contact angles of oil on the Teflon-coated surfaces indicate better affinity and wettability of the perfluorinated oil on the Teflon-coated hydrophobic surfaces than on a bare aluminum or aluminum oxide surfaces. In addition, since the Teflon-coated AAO layer has the disconnected dead-end nanopores (70 nm in diameter) and good affinity with the perfluorinated oil, the capillary force maintaining the oil inside of the nanoscale dead-end pores should be extremely large, which enables the AAO layer to strongly retain the oil within the pores[37]. The high-aspect-ratio dead-end nanoporous geometry also contributes to a disjoining pressure causing the oil in the pores to be under negative pressure, so that the evaporation of oil can be impeded in the nanopores of the AAO layer.[38]

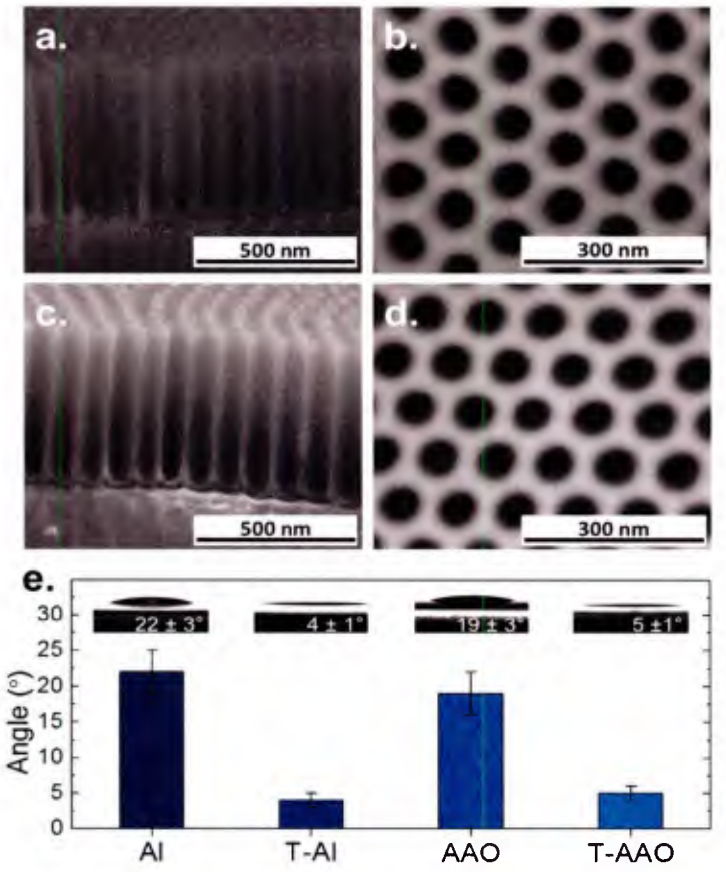

Figure 2. SEM images of (a) the cross-section and (b) the top view of the AAO layer before Teflon coating, and (c) the cross-section and (d) the top view of the AAO layer after Teflon coating, respectively. (e) Apparent contact angles of oil droplets (Krytox GPL 100) on the bare AAO and the Teflon-coated AAO (T-AAO) compared to bare aluminum (Al) and the Teflon-coated aluminum (T-Al).

Despite the good wettability of oil on the Teflon-coated AAO surface, it is not guaranteed that the oil will fully replace the air residing in the pores and penetrate to the bottom of the pores because of the high-aspect-ratio dead-end geometry of the pores and the low air solubility of oil.[39-41] To address this issue, we have developed a solvent exchange method that allows the complete penetration of the oil into the pores. This method involves sequential exchange of solvents, starting from ethanol, which can easily penetrate the pore owing to its low surface tension and low Henry's law constant. Then, the ethanol is replaced with Vertrel XF, which is miscible with both the ethanol and the oil (Krytox GPL 100). Finally, Vertrel XF is replaced with oil so that the pores contain only the oil.

To verify the full imbibition of the oil in the nanopores of the AAO layer, we have mixed curable photoresist solution into Vertrel XF (solvent for oil) so that the solution can be solidified and thus can be visualized with SEM. **Figure 3** shows the SEM images of the cross-sections of the AAO layers after imbibition of the Vertrel XF-photoresist mixture. In the case of the Teflon-coated AAO with no oil impregnation (i.e., just air-filled empty nanopores),

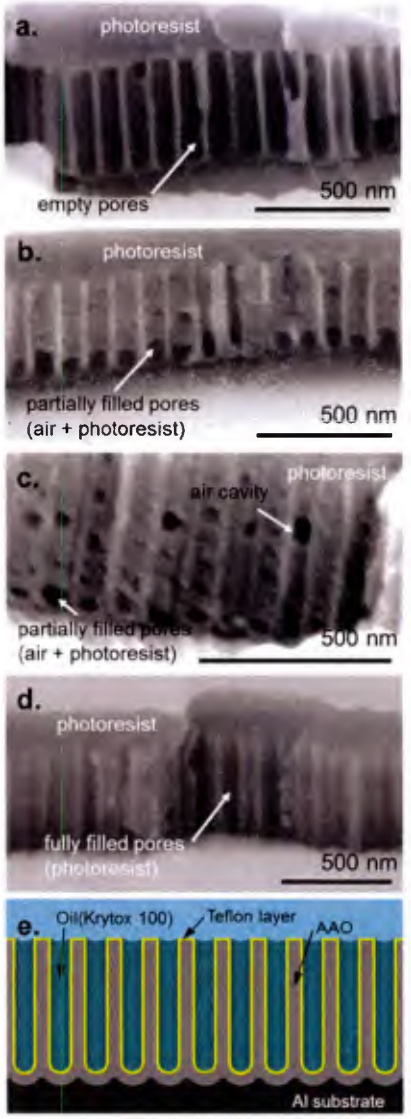

Figure 3. SEM images of the cross-section of the Teflon-coated AAO (T-AAO) layers after the imbibition test of the mixture of Vertrel XF and photoresist polymer. (a) T-AAO with empty pores. (b) T-AAO with oil impregnation by immersing in oil for 24 hours. (c) T-AAO with oil impregnation by immersing in oil for 20 minutes with ultrasonication. (d) T-AAO with oil impregnation by the solvent exchange method developed. (e) Schematic of the cross-section of the completely oil-impregnated Teflon-coated AAO.

the mixture did not penetrate the pores and instead the solidified photoresist material only covers the top surface of the AAO layer (**Figure 3a**). In the case of the Teflon-coated AAO with oil impregnation achieved simply by dipping in the oil for 24 hours, the mixture penetrates the pores, but air still remained at the bottom of pores, indicating that the oil did not fully penetrate the pores (**Figure 3b**). Several air cavities were also observed along the partially filled pores, indicating that the pores were not continuously filled by the oil. The ultrasonication for 20 minutes was also applied in the simple dipping process to compare with the solvent exchange method. The result (**Figure 3c**) shows the ultrasonication helped the mixture to penetrate more into the pores. However, air (despite less amount) remained at the bottom of pores, and air cavities were also observed along the pores, indicating that the simple dipping was not capable of continuous and full infiltration of the oil into the nanopores. In contrast, in the case of the Teflon-coated AAO with oil impregnation by the solvent exchange method developed (**Figure 3d**), the photoresist material completely fills the nanopores and no air pockets are found at the bottom of pores, implying that oil completely fills the pores via the solvent-exchange method (**Figure 3e**).

2.2. Corrosion resistance of oil-impregnated nanoporous oxide layer on aluminum

We have evaluated the anti-corrosion performance of the oil-impregnated Teflon-coated AAO (O-T-AAO) surface using electrochemical impedance spectroscopy (EIS), compared with Al, AAO, T-AAO, and oil-impregnated AAO (O-AAO) surfaces. **Figures 4a** and **4b** first show the impedance (|Z|) and phase (°) on a Bode plot, respectively, obtained using a simplified equivalent circuit as shown in **Figure 4c**. As a result of the model fitting, $R_{barrier}$ (resistance of a barrier layer) and $C_{barrier}$ (capacitance of a barrier layer) of the surfaces are plotted as shown in **Figure 4d**. A higher value of $R_{barrier}$ implies higher corrosion resistance to the corrosive media (1 M HCl solution).[43] From the fact that the samples used in this work have different wettabilities, the different $R_{barrier}$ values result from the different wetting behaviors of the corrosive media (1 M HCl solution in water) on the surfaces. Imbibition of water into the bare AAO, which is hydrophilic, is much easier than with the hydrophobic T-AAO. Therefore, the pores of the bare AAO are more likely to be filled with the corrosive media than those of T-AAO, giving the surface a greater number of corrosion sites. The results indeed show this characteristic since

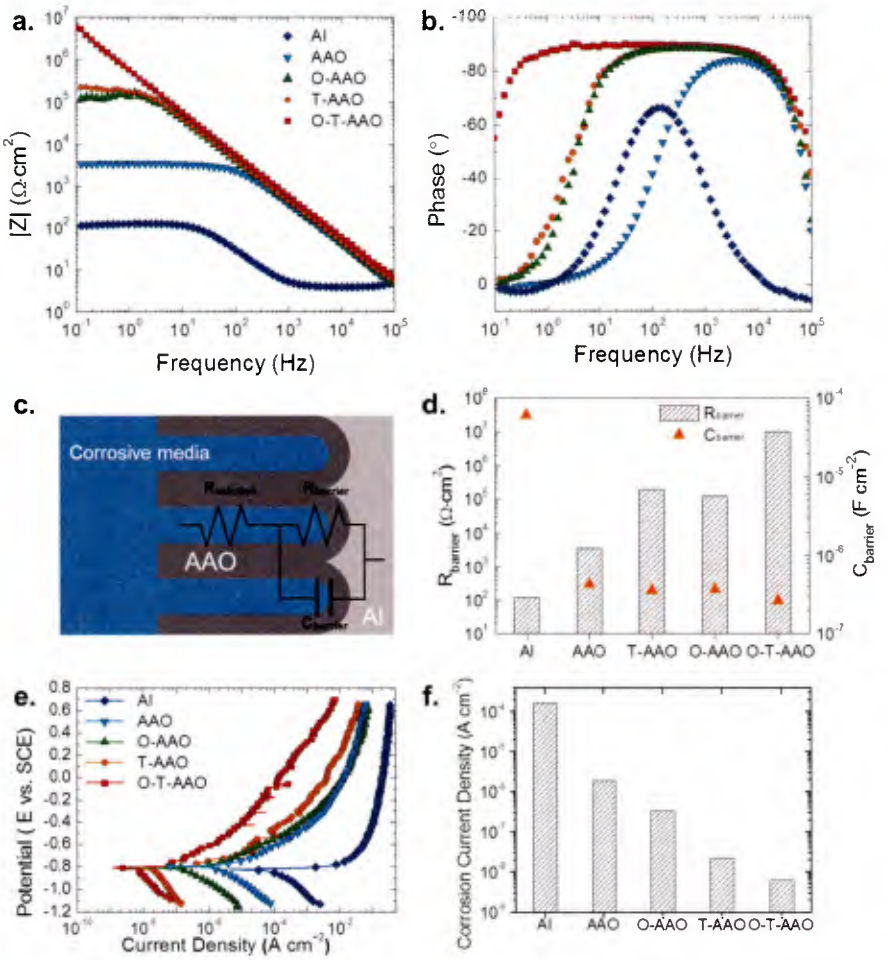

Figure 4. Electrochemical impedance spectroscopy (EIS) measured in 1 M HCl solution. (a) Impedance (|Z|) and (b) phase on a Bode plot for bare aluminum (Al), anodic aluminum oxide (AAO), Teflon-coated AAO (T-AAO), oil-impregnated AAO (O-AAO), and oil-impregnated Teflon-coated AAO (O-T-AAO). (c) Equivalent circuit for model fitting. (d) Resistance and capacitance of the barrier layer for each surface obtained from the model fitting. (e) Potentiodynamic polarization curves measured in 1 M HCl solution. (f) Corrosion current density calculated by Tafel fitting obtained from the potentiodynamic polarization data.

the resistance of the bare AAO ($R_{barrier}^{AAO}$ = 3.45 × 10^3 Ω·cm^2) is much lower than that of the T-AAO ($R_{barrier}^{T-AAO}$ = 1.97 × 10^5 Ω·cm^2). Eventually, the $R_{barrier}$ value reflects how many pores are filled with corrosive media, implying a resistance against the corrosion under the aqueous environment.

In the same manner, a higher value of capacitance was obtained by the greater area of corrosion reaction (i.e., corrosion sites), indicating the lower value of the resistance of the bare AAO as a barrier layer. Meanwhile, despite the increase of the area of corrosion sites due to the porous geometry, the $R_{barrier}$ value of AAO (3.45 × 10^3 Ω·cm^2) was still larger than that of Al (1.18 × 10^2 Ω·cm^2), which is due to the passivating oxide layer in the case of AAO. In the case of O-AAO surface, the $R_{barrier}$ value was 1.23 × 10^5 Ω·cm^2, which is also much greater than that of AAO (3.45 × 10^3 Ω·cm^2). Significantly increased $R_{barrier}$ by the oil impregnation into bare AAO (O-AAO) implies that the oil should be entrained in the pores to inhibit the penetration of corrosive media into the pores. However, the $R_{barrier}$ value of the O-AAO surface (1.23 × 10^5 Ω·cm^2) was slightly lower than that of T-AAO (1.97 × 10^5 Ω·cm^2). In the case of O-T-AAO, the $R_{barrier}$ value was most significantly increased, up to 1.03 × 10^7 Ω·cm^2, which is two orders of magnitude higher than that of T-AAO or O-AAO, and four orders of magnitude greater than that of the bare AAO. This result indicates that the corrosive media is fully separated from the AAO surface by the oil layer (O) which is more stably retained on the surface than in the case of O-AAO, due to the hydrophobic Teflon layer (T) pre-applied on the AAO surface. The result also indicates that the hydrophobic Teflon coating is

important to have good and stable oil impregnation into the pore structures of the AAO layer. Also, the result indicates that the oil layer impregnated in the case of the O-T-AAO surface is more effective than the air layer impregnated in the case of T-AAO for corrosion inhibition.

Anti-corrosion performance of the O-T-AAO surface was further evaluated using a potentiodynamic polarization method. **Figure 4e** shows the potentiodynamic polarization curves obtained in 1 M HCl solution and **Figure 4f** the corrosion current densities calculated by Tafel fitting[44-45] of the obtained curves. The O-T-AAO shows the lowest value of corrosion current density, up to 6.25×10^{-9} A cm^{-2}, which is 3.5 times lower than T-AAO (2.21×10^{-8} A cm^{-2}), and three orders of magnitude lower than bare AAO (1.89×10^{-6} A cm^{-2}). In addition, the O-T-AAO shows the highest *IE* value, up to 99.99%, which implies excellent corrosion resistance, which is attributed to the superior water repellency resulting from the stable oil layer impregnated into the hydrophobic (i.e., Teflon-coated) nanopores. These results are in good agreement with the EIS results where the highest $R_{barrier}$ value was measured for O-T-AAO, and confirm again that the oil impregnated nanopores is more effective to inhibit the corrosion than the air impregnated hydrophobic surface.

2.3. Self-healing capability of oil-impregnated nanoporous oxide layer on aluminum

Surface damage of a coating layer is regarded as a fatal issue for anti-corrosive surface treatments, including anodization, since the metal surfaces are likely to be exposed after being damaged. In this regard, developing an anti-corrosive coating that can autonomously recover the damaged area and so provide an anti-corrosion capability is of great interest. The proposed oil-impregnated surface allows this feature as the impregnated liquid oil can immediately flow and cover the exposed area upon damage. To evaluate the corrosion tolerance to such surface damage, we deliberately created cracks in the AAO layer by bending the AAO samples (T-AAO and O-T-AAO) against a cylindrical tube (diameter 2 cm), as shown in **Figure 5a**. The cracks in the AAO layer cause the underlying aluminum substrate to be exposed to the external environment (**Figure 5b**). After the cracks were generated, where most of the cracks are formed perpendicular to the bending direction, the samples were flattened back. As shown in **Figure 5c**, the cracks were still evident even after being flattened back, causing the underlying aluminum substrate to be exposed to the corrosive media.

The corrosion resistances of the bent T-AAO and O-T-AAO samples (named B-T-AAO and B-O-T-AAO, respectively) were evaluated by potentiodynamic polarization measurements in 1M HCl solution. The results of the potentiodynamic polarization measurement and the corrosion current densities for B-T-AAO and B-O-T-AAO, compared with T-AAO and O-T-AAO, as well as bare Al, are shown in **Figures 5d** and **5e**, respectively. After the cracks were generated on the AAO layers, the corrosion current densities for both samples (B-T-AAO and B-O-T-AAO) were increased compared to the intact AAO layers (T-AAO and O-T-AAO), which suggests that some portion of the aluminum surface was exposed to the corrosive media due to the cracks[12, 21]. However, it should be noted that the corrosion current density of the B-O-T-AAO surface was increased only by a factor of 4 (from 6.25×10^{-9} to 2.88×10^{-8} A cm^{-2}), whereas the corrosion current density of the B-T-AAO surface increased by more than 30 times (from 2.21×10^{-8} to 6.68×10^{-7} A cm^{-2}). In addition, due to the presence of cracks in AAO, the *IE* value of T-AAO decreases by 0.39 %, while the decrease is much less (only by 0.01 %) for O-T-AAO. The reason for such a dramatic difference between B-O-T-AAO and B-T-AAO is mainly because the oil impregnated in the B-O-T-AAO can flow towards the damaged region and cover the exposed area to protect

against the corrosive media. Moreover, the current density of the B-T-AAO increased more rapidly in the anodic potential region and finally was comparably close to that of Al, showing how vulnerable the T-AAO surface is against surface damage. Although the corrosion current density of the B-O-T-AAO was slightly higher than that of T-AAO, the current density at the anodic potential region is still significantly lower (**Figure 5d**).

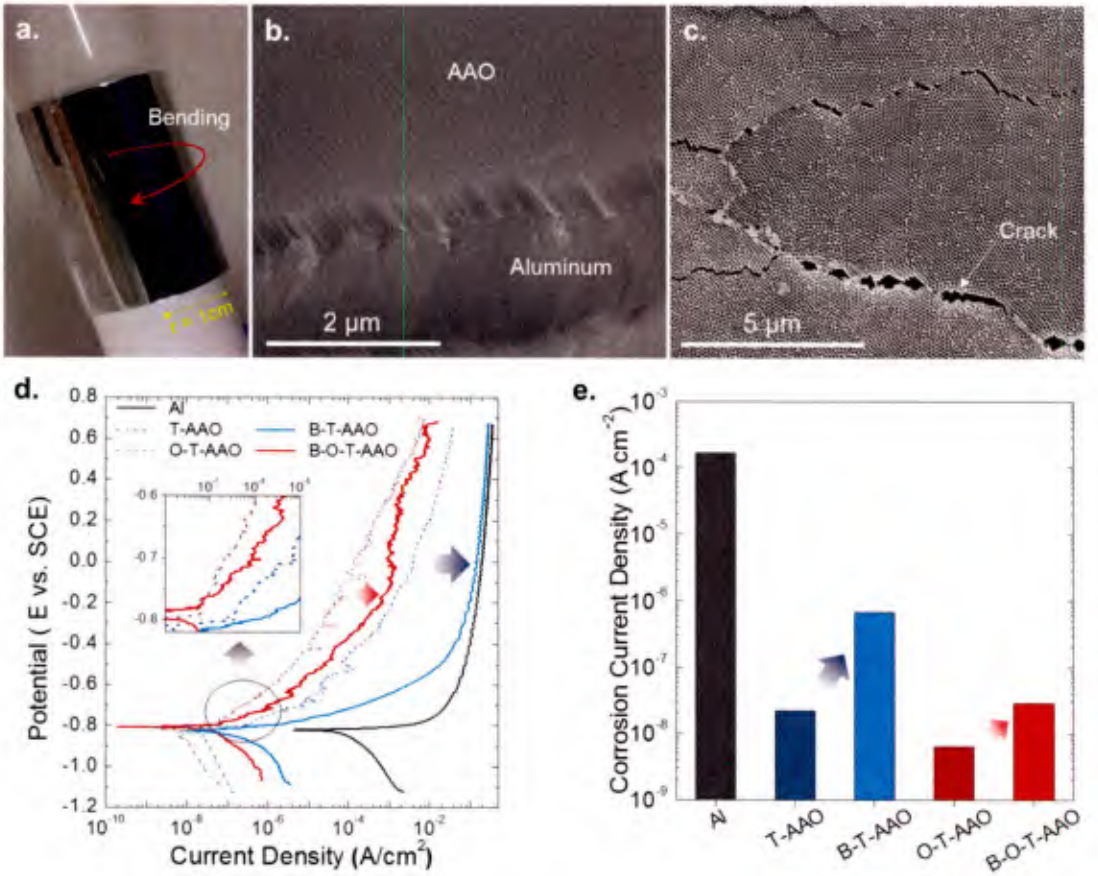

Figure 5. Crack in the AAO layer and the evaluation of corrosion tolerance to the surface damage. (a) Cracks are generated by bending a sample against a cylindrical pipe (diameter 2 cm). (b) SEM image showing the bottom aluminum surface exposed due to the crack by bending of a sample (T-AAO). (c) SEM images of cracks generated on the sample (T-AAO) by the bending and flattening. (d) Potentiodynamic polarization measurement results of the damaged samples (B-T-AAO and B-O-T-AAO), compared to the original samples (T-AAO and O-T-AAO) as well as Al, conducted in 1 M HCl solution. (e) Corrosion current density obtained from the potentiodynamic polarization data.

To visually demonstrate the advantage of the self-healing property for anti-corrosion, a highly corrosive liquid (35 wt. % HCl + saturated $CuSO_4$) was placed on the B-O-T-AAO and B-T-AAO surfaces, respectively, which contain many defects and cracks. Appearances of the corrosive liquid droplet on the surfaces over time are shown in **Figure 6**. For the B-O-T-AAO surfaces, O-T-AAOs prepared by a simple dip coating as wells by the solvent exchange method for the oil impregnation were tested to verify the significance of the complete impregnation of oil into the high-aspect-ratio dead-end nanopores for the superior self-healing property. Prior to bending the O-T-AAOs for crack, a shear flow of water was applied for 5 min on both surfaces.

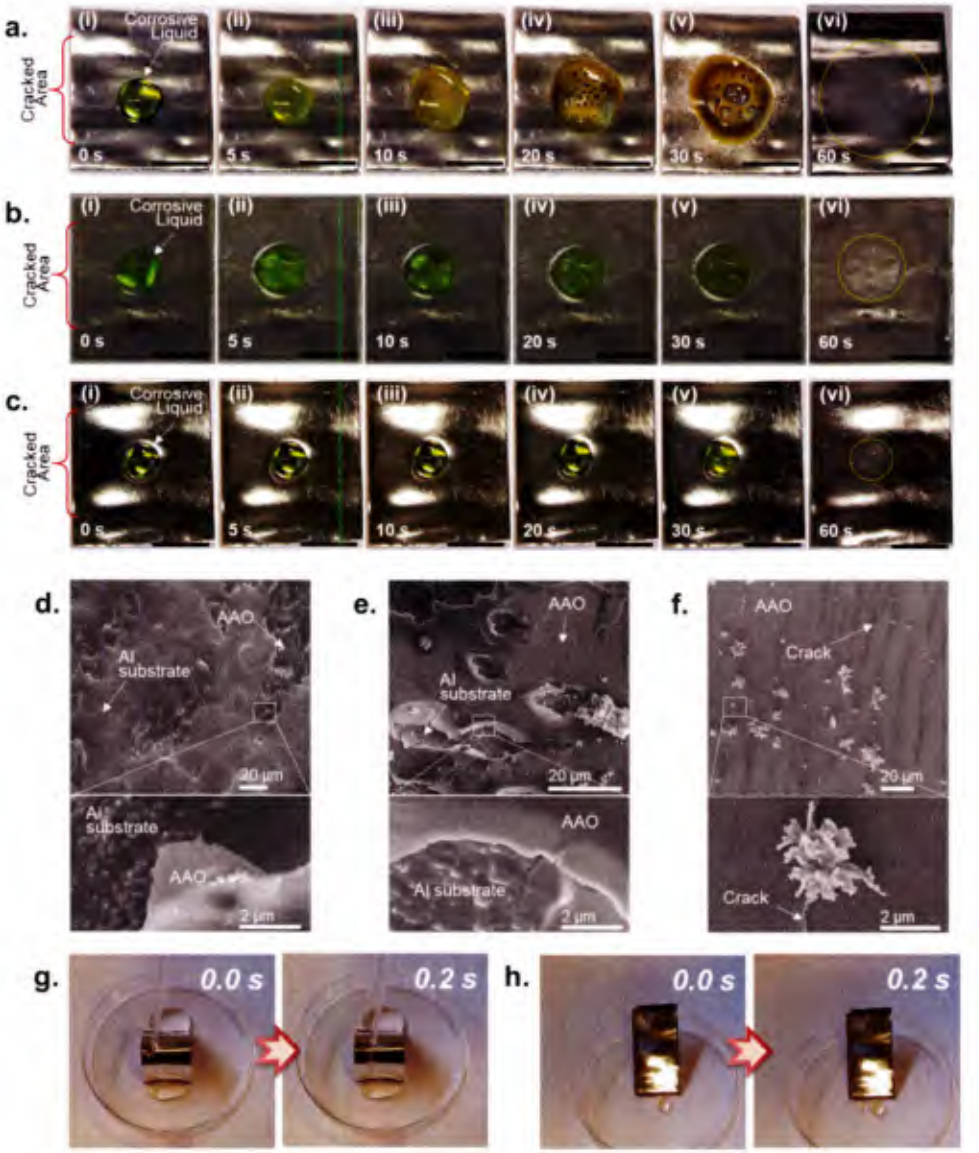

Figure 6. (a-c) Sequential images of a highly corrosive liquid droplet (35 wt. % HCl + saturated $CuSO_4$) sitting on the surfaces of (a) B-T-AAO, (b) B-O-T-AAO prepared with a simple dip coating method, and (c) B-O-T-AAO prepared with the solvent exchange method; (i)-(v) sequential images and (vi) after 60 seconds when the corrosive liquid droplet was removed by dipping in water. Prior to bending for crack, a shear flow of water was applied on the O-T-AAOs (both b and c) for 5 minutes. The scale bar in each image in (a), (b), and (c) indicates 1 cm. (d-f) Close-up SEM images of the corrosion marks (the circular areas marked in (a-vi), (b-vi), and (c-vi)) on the B-T-AAO and B-O-T-AAO surfaces. Sequential images of a water droplet on (g) B-O-T-AAO and (h) its surface flattened back.

The corrosive liquid droplet on the B-T-AAO surface (**Figure 6a**) rapidly spread out due to the significant evolution of gas caused by the dissolution of aluminum, indicating a high corrosion rate of the B-T-AAO. The B-O-T-AAO prepared with a simple dip coating method for the oil impregnation also shows the significant evolution of gas with enlarging droplet (**Figure 6b**). In contrast, the corrosive liquid droplet on the B-O-T-AAO prepared with the solvent exchange method (**Figure 6c**) slowly slid along the surface, and there was no gas evolution and

noticeable change to the corrosive liquid droplet, indicating a significantly impeded corrosion. The corrosive liquid droplet left a mark of corrosion for all surfaces. However, the mark on B-O-T-AAO prepared with the solvent exchange method was significantly smaller than that on the B-T-AAO as well as the B-O-T-AAO prepared with a conventional dip coating method. Microstructures of the surface area of each corrosion mark are shown for B-T-AAO and B-O-T-AAOs in **Figures 6d**, **6e**, and **6f**, respectively. In case of the B-T-AAO (**Figure 6d**) and the B-O-T-AAO prepared with a conventional dip coating for the oil impregnation (**Figure 6e**), most of the AAO layer has been removed by severe corrosion, thus the initial cracks in the AAO were not observable. In addition, the dissolved aluminum surface without an AAO layer was revealed to the outside. In contrast, the microstructures of the B-O-T-AAO layer prepared with the solvent exchange method for the oil impregnation were not significantly damaged by the corrosive liquid droplet so that any aluminum substrate underneath of the AAO layer was not revealed. Only the copper residues formed by the displacement reaction with dissolved aluminum were found on some cracks (**Figure 6f**), indicating that the corrosive media could not spread along the cracks. The results indicate that O-T-AAO realized with the solvent exchange method for the oil impregnation has an exceptional corrosion tolerance to physical damage and defects on the surface in such a way that the oil impregnated in the pores can wick into the cracked region and fill the cracks. Hence, the oil automatically re-covers the exposed metallic aluminum surface, insulating aluminum from the external corrosive environment. Nonetheless, the superior self-healing capability of the oil-impregnated Teflon-coated AAO (O-T-AAO) enabled by the solvent exchange method, which allows a durable and robust anti-corrosion behavior, is the most distinguished property compared to the hydrophobic AAO (T-AAO). Since the oil covers the damaged areas in the O-T-AAO surface, the irregular cracks do not become pinning sites for a water droplet so that the surface still slippery (**Figures 6g** and **6h**).

3. CONCLUSIONS

We have developed a solvent exchange method that allows the full impregnation of oil into high-aspect-ratio dead-end nanopores of an anodic aluminum oxide layer fabricated on an aluminum substrate. The synergetic effect of a hydrophobic Teflon coating followed by the oil impregnation has established a highly robust and stable non-wetting surface against water on the AAO layer. The fully and stably entrained oil in the Teflon-coated hydrophobic nanopores of the AAO layer has significantly enhanced the corrosion resistance of aluminum by inhibiting the penetration of corrosive aqueous media into the pores. The impregnated liquid oil can wick into damaged sites such as cracks in the AAO layer, further preventing the exposure of aluminum surface to the outer environments and thus corrosion. Such superior corrosion resistance and damage tolerance for corrosion with a unique self-healing capability of the oil-impregnated hydrophobic nanoporous AAO, compared to the only air-entrained hydrophobic nanoporous AAO, is due to the liquid oil having effectively impregnated the high-aspect-ratio dead-end nanopores using the newly developed solvent exchange method. The oil-impregnated nanoporous oxide surface with the great durability in retaining the liquid oil layer within the surface and the self-healing capability will be of great significance not only in the corrosion protection for metallic substrates but also many other applications such as anti-icing, anti-biofouling, and self-cleaning, for naval systems.

REFERENCES

1. Foley, R. T., Localized Corrosion of Aluminum Alloys—A Review. *Corrosion* **1986,** *42* (5), 277-288.

2. Wu, L.-K.; Liu, L.; Li, J.; Hu, J.-M.; Zhang, J.-Q.; Cao, C.-N., Electrodeposition of cerium (III)-modified bis-[triethoxysilypropyl]tetra-sulphide films on AA2024-T3 (aluminum alloy) for corrosion protection. *Surface and Coatings Technology* **2010,** *204* (23), 3920-3926.

3. Simões, A. M.; Battocchi, D.; Tallman, D. E.; Bierwagen, G. P., SVET and SECM imaging of cathodic protection of aluminium by a Mg-rich coating. *Corrosion Science* **2007,** *49* (10), 3838-3849.

4. Hu, J.-M.; Liu, L.; Zhang, J.-Q.; Cao, C.-N., Electrodeposition of silane films on aluminum alloys for corrosion protection. *Progress in Organic Coatings* **2007,** *58* (4), 265-271.

5. Grundmeier, G.; Schmidt, W.; Stratmann, M., Corrosion protection by organic coatings: electrochemical mechanism and novel methods of investigation. *Electrochim. Acta* **2000,** *45* (15–16), 2515-2533.

6. Cohen, S. M., Review: Replacements for Chromium Pretreatments on Aluminum. *Corrosion* **1995,** *51* (1), 71-78.

7. Diggle, J. W.; Downie, T. C.; Goulding, C. W., Anodic oxide films on aluminum. *Chemical Reviews* **1969,** *69* (3), 365-405.

8. Lee, W.; Ji, R.; Gosele, U.; Nielsch, K., Fast fabrication of long-range ordered porous alumina membranes by hard anodization. *Nat Mater* **2006,** *5* (9), 741-747.

9. Thompson, G. E.; Wood, G. C., Porous anodic film formation on aluminium. *Nature* **1981,** *290* (5803), 230-232.

10. Thompson, G. E.; Furneaux, R. C.; Wood, G. C.; Richardson, J. A.; Goode, J. S., Nucleation and growth of porous anodic films on aluminium. *Nature* **1978,** *272* (5652), 433-435.

11. Lee, J.; Jung, U.; Kim, W.; Chung, W., Effects of residual water in the pores of aluminum anodic oxide layers prior to sealing on corrosion resistance. *Applied Surface Science* **2013,** *283*, 941-946.

12. Huang, Y.; Shih, H.; Huang, H.; Daugherty, J.; Wu, S.; Ramanathan, S.; Chang, C.; Mansfeld, F., Evaluation of the corrosion resistance of anodized aluminum 6061 using electrochemical impedance spectroscopy (EIS). *Corrosion Science* **2008,** *50* (12), 3569-3575.

13. Moutarlier, V.; Gigandet, M. P.; Normand, B.; Pagetti, J., EIS characterisation of anodic films formed on 2024 aluminium alloy, in sulphuric acid containing molybdate or permanganate species. *Corrosion Science* **2005,** *47* (4), 937-951.

14. Lu, Z.; Wang, P.; Zhang, D., Super-Hydrophobic Film Fabricated on Aluminium Surface as a Barrier to Atmospheric Corrosion in a Marine Environment. *Corrosion Science* **2015,** *91*, 287-296.

15. Jeong, C.; Lee, J.; Sheppard, K.; Choi, C.-H., Air-Impregnated Nanoporous Anodic Aluminum Oxide Layers for Enhancing the Corrosion Resistance of Aluminum. *Langmuir* **2015,** *31* (40), 11040-11050.

16. Wang, P.; Zhang, D.; Qiu, R.; Wan, Y.; Wu, J., Green approach to fabrication of a super-hydrophobic film on copper and the consequent corrosion resistance. *Corrosion Science* **2014,** *80* (0), 366-373.

17. Ishizaki, T.; Masuda, Y.; Sakamoto, M., Corrosion Resistance and Durability of Superhydrophobic Surface Formed on Magnesium Alloy Coated with Nanostructured Cerium Oxide Film and Fluoroalkylsilane Molecules in Corrosive NaCl Aqueous Solution. *Langmuir* **2011,** *27* (8), 4780-4788.

18. Liu, T.; Chen, S. G.; Cheng, S.; Tian, J. T.; Chang, X. T.; Yin, Y. S., Corrosion behavior of super-hydrophobic surface on copper in seawater. *Electrochim. Acta* **2007,** *52* (28), 8003-8007.

19. Lee, W.; Park, B. G.; Kim, D. H.; Ahn, D. J.; Park, Y.; Lee, S. H.; Lee, K. B., Nanostructure-Dependent Water-Droplet Adhesiveness Change in Superhydrophobic Anodic Aluminum Oxide Surfaces: From Highly Adhesive to Self-Cleanable. *Langmuir* **2010,** *26* (3), 1412-1415.

20. Aljallis, E.; Sarshar, M. A.; Datla, R.; Sikka, V.; Jones, A.; Choi, C.-H., Experimental Study of Skin Friction Drag Reduction on Superhydrophobic Flat Plates in High Reynolds Number Boundary Layer Flow. *Physics of Fluids* **2013,** *25* (2), 025103.

21. Herrera-Hernandez, H.; Vargas-Garcia, J. R.; Hallen-Lopez, J. M.; Mansfeld, F., Evaluation of different sealing methods for anodized aluminum-silicon carbide (Al/SiC) composites using EIS and SEM techniques. *Materials and Corrosion* **2007,** *58* (11), 825-832.

22. Tian, Z.; Yu, H.; Wang, L.; Saleem, M.; Ren, F.; Ren, P.; Chen, Y.; Sun, R.; Sun, Y.; Huang, L., Recent progress in the preparation of polyaniline nanostructures and their applications in anticorrosive coatings. *RSC Advances* **2014,** *4* (54), 28195-28208.

23. Solomon, B. R.; Khalil, K. S.; Varanasi, K. K., Drag Reduction using Lubricant-Impregnated Surfaces in Viscous Laminar Flow. *Langmuir* **2014,** *30* (36), 10970-10976.

24. Vogel, N.; Belisle, R. A.; Hatton, B.; Wong, T. S.; Aizenberg, J., Transparency and Damage Tolerance of Patternable Omniphobic Lubricated Surfaces Based on Inverse Colloidal Monolayers. *Nat. Commun.* **2013,** *4*, 10.

25. Rykaczewski, K.; Anand, S.; Subramanyam, S. B.; Varanasi, K. K., Mechanism of Frost Formation on Lubricant-Impregnated Surfaces. *Langmuir* **2013,** *29* (17), 5230-5238.

26. Epstein, A. K.; Wong, T. S.; Belisle, R. A.; Boggs, E. M.; Aizenberg, J., Liquid-Infused Structured Surfaces with Exceptional Anti-Biofouling Performance. *Proceedings of the National Academy of Sciences* **2012,** *109* (33), 13182-13187.

27. Kim, P.; Wong, T.-S.; Alvarenga, J.; Kreder, M. J.; Adorno-Martinez, W. E.; Aizenberg, J., Liquid-Infused Nanostructured Surfaces with Extreme Anti-Ice and Anti-Frost Performance. *ACS Nano* **2012,** *6* (8), 6569-6577.

28. Anand, S.; Paxson, A. T.; Dhiman, R.; Smith, J. D.; Varanasi, K. K., Enhanced Condensation on Lubricant-Impregnated Nanotextured Surfaces. *ACS Nano* **2012,** *6* (11), 10122-10129.

29. Wong, T.-S.; Kang, S. H.; Tang, S. K. Y.; Smythe, E. J.; Hatton, B. D.; Grinthal, A.; Aizenberg, J., Bioinspired Self-repairing Slippery Surfaces with Pressure-Stable Omniphobicity. *Nature* **2011,** *477* (7365), 443-447.

30. Jeong, C.; Choi, C.-H., Single-Step Direct Fabrication of Pillar-on-Pore Hybrid Nanostructures in Anodizing Aluminum for Superior Superhydrophobic Efficiency. *ACS Applied Materials & Interfaces* **2012,** *4* (2), 842-848.

31. Yao, X.; Song, Y.; Jiang, L., Applications of Bio-Inspired Special Wettable Surfaces. *Adv. Mater.* **2011,** *23* (6), 719-734.

32. Zhang, L.; Zhou, Z.; Cheng, B.; DeSimone, J. M.; Samulski, E. T., Superhydrophobic Behavior of a Perfluoropolyether Lotus-Leaf-like Topography. *Langmuir* **2006,** *22* (20), 8576-8580.

33. Lee, C.; Kim, A.; Kim, J., Electrochemically etched porous stainless steel for enhanced oil retention. *Surface and Coatings Technology* **2015,** *264*, 127-131.

34. Sunny, S.; Vogel, N.; Howell, C.; Vu, T. L.; Aizenberg, J., Lubricant-Infused Nanoparticulate Coatings Assembled by Layer-by-Layer Deposition. *Advanced Functional Materials* **2014,** *24* (42), 6658-6667.

35. Smith, J. D.; Dhiman, R.; Anand, S.; Reza-Garduno, E.; Cohen, R. E.; McKinley, G. H.; Varanasi, K. K., Droplet Mobility on Lubricant-Impregnated Surfaces. *Soft Matter* **2013,** *9* (6), 1772-1780.

36. Rykaczewski, K.; Landin, T.; Walker, M. L.; Scott, J. H. J.; Varanasi, K. K., Direct Imaging of Complex Nano- to Microscale Interfaces Involving Solid, Liquid, and Gas Phases. *ACS Nano* **2012,** *6* (10), 9326-9334.

37. Zhmud, B. V.; Tiberg, F.; Hallstensson, K., Dynamics of Capillary Rise. *Journal of Colloid and Interface Science* **2000,** *228* (2), 263-269.

38. Maroo, S. C.; Chung, J., Negative pressure characteristics of an evaporating meniscus at nanoscale. *Nanoscale Research Letters* **2011,** *6* (1), 72.

39. Phan, V. N.; Joseph, P.; Djeghlaf, L.; Allouch, A. E. D.; Bourrier, D.; Abgrall, P.; Gué, A.-M.; Yang, C.; Nguyen, N.-T., Capillary Filling in Nanochannels—Modeling, Fabrication, and Experiments. *Heat Transfer Engineering* **2011,** *32* (7-8), 624-635.

40. Phan, V. N.; Nguyen, N.-T.; Yang, C.; Joseph, P.; Djeghlaf, L.; Bourrier, D.; Gue, A.-M., Capillary Filling in Closed End Nanochannels. *Langmuir* **2010,** *26* (16), 13251-13255.

41. Pray, H. A.; Schweickert, C. E.; Minnich, B. H., Solubility of Hydrogen, Oxygen, Nitrogen, and Helium in Water at Elevated Temperatures. *Industrial & Engineering Chemistry* **1952,** *44* (5), 1146-1151.

42. Sieverts, A., Absorption of gases by metals. *Zeitschrift für Metallkunde* **1929,** *21*, 37-46.

43. Lopez, V.; Gonzalez, J. A.; Otero, E.; Escudero, E.; Morcillo, M., Atmospheric corrosion of bare and anodised aluminium in a wide range of environmental conditions. Part II: Electrochemical responses. *Surf. Coat. Technol.* **2002,** *153* (2-3), 235-244.

44. Mansfeld, F., Simultaneous Determination of Instantaneous Corrosion Rates and Tafel Slopes from Polarization Resistance Measurements. *J. Electrochem. Soc.* **1973,** *120* (4), 515-518.

45. Mansfeld, F., Tafel Slopes and Corrosion Rates from Polarization Resistance Measurements. *Corrosion* **1973,** *29* (10), 397-402.